Transp Porous Med (2007) 70:127–146
DOI 10.1007/s11242-006-9088-x

ORIGINAL PAPER

Fluid flow properties for different classes of intermediate wettability as studied by network modelling

Linda Kåda Høiland · Kristine Spildo · Arne Skauge

Received: 6 April 2005 / Accepted: 7 November 2006 / Published online: 1 February 2007

Abstract Most clastic reservoirs display an intermediate type of wettability. Intermediate wettability covers several local wetting configurations like fractional wet and mixed-wet where the oil-wet sites could either be in the large or smaller pores. Clastic reservoirs show a large variation in fluid flow properties. A classical invasion–percolation network simulator is used to investigate properties of different intermediate wet situations. Variation in wetting properties like contact angles, process dependent contact angles, contact angle distribution, and fraction of oil wet sites are investigated. The fluid flow properties analysed in particular are residual oil saturation and normalized endpoint relative permeability. Results from network modelling have been compared to reservoir core analysis data. The network models applied are at the capillary limit, while the core flood results are clearly viscous influenced. Even though network modelling does not cover all the physics involved in fluid displacement processes, results show that data from simulations are sufficient to present trends in fluid flow properties which are comparable to experimental data.

Keywords Intermediate wettability · Amott–Harvey · USBM · Oil-Wet fraction · Contact angle hysteresis · Residual oil saturation

Nomenclature

Sor	Residual oil saturation
Swi	Irreducible water saturation
Krw(Sor)	End-point relative permeability
MWL	Mixed wet large
FW	Fractional wet
MWS	Mixed wet small
I_o	Oil wettability index
I_w	Water wettability index

L. K. Høiland · K. Spildo (✉)· A. Skauge
Center for Integrated Petroleum Research, Allègaten 41, 5007 Bergen, Norway
e-mail: Kristine.Spildo@cipr.uib.no

I_{AH}	Amott Harvey wettability index (I_w–I_o)
I_{USBM}	USBM wettability index
α	Oil-wet fraction
α_{num}	Oil-wet fraction by number
α_{vol}	Oil-wet fraction by volume
α_{crit}	Critical oil-wet fraction
$\alpha_{num,crit}$	Critical oil-wet fraction by number
$\alpha_{vol,crit}$	Critical oil-wet fraction by number
θ	Contact angle
θ_{ww}	Contact angle in the water-wet pores
θ_{ow}	Contact angle in the oil-wet pores
θ_a	Advancing contact angle
θ_{cw}	Critical water-wet contact angle
θ_{co}	Critical oil-wet contact angle
r	Radius
σ_{ow}	Interfacial tension between oil and water
β	Angle of pore corner
P_c	Capillary pressure
P_o	Pressure oil phase
P_w	Pressure water phase
A_i	Arbitrary numbers
x_i	Random number between 0 and 1
ΔS_{ws}	Change in water saturation during spontaneous water imbibition
ΔS_{wf}	Change in water saturation during forced water imbibition
ΔS_{os}	Change in oil saturation during spontaneous oil imbibition
ΔS_{of}	Change in oil saturation during forced water imbibition
A	Area under curve
D	Network dimension
z	Co-ordination number

1 Introduction

Wettability is known to play a major role in fluid flow and displacement processes in porous media. However, no direct measurement of the wettability of porous media is available. Instead the most widely used empirical wettability measurements for reservoir cores are based on displacement studies. Examples include the Amott–Harvey (Amott 1959; Boeneau and Clampitt 1977) and USBM (Donaldson et al. 1969) wettability tests.

Most reservoirs are neither strongly water-wet nor strongly oil-wet, but fall in between these two extremes. This large group of intermediate-wet state includes reservoirs with neutral and close to neutral wettability indices (AH and USBM). Special core analysis of intermediate-wet rock shows a large scatter in properties such as residual oil saturation (Sor), relative permeability and capillary pressure. We have earlier pursued an approach to improve the understanding of the intermediate-wet state by dividing this group into three sub-classes (Skauge and Ottesen 2002; Skauge et al. 2003) as first proposed by Dixit et al. (1998); fractional-wet (FW), where oil- and water-wet sites are random with respect to pore size, and two mixed-wet classes defined by water- and oil-wet sites that are sorted by pore size. The mixed-wet large

(MWL) class is characterized by the large pores being oil-wet, while mixed-wet small (MWS) refers to a situation where small pores are oil-wet (see Fig. 1). The existence of these three different classes of intermediate wettability was later verified both theoretically and experimentally (Skauge et al. 2006).

To distinguish between the different intermediate-wet states, Skauge and Ottesen (2002) and Skauge et al. (2003) used an approach based on network model studies by Dixit et al. (1998). The studies by Dixit et al. indicate that one may distinguish between these intermediate-wet classes based on the relationship between the Amott–Harvey (I_{AH}) and USBM (I_{USBM}) wettability indices. While I_{AH} and I_{USBM} are almost equal for the FW class, I_{USBM} is larger than I_{AH} for the MWL class and smaller than I_{AH} for the MWS class (see Fig. 2). Using this classification method, it was demonstrated that the three different intermediate wetting states can be identified from reservoir core data if both the Amott–Harvey and USBM wettability indices are known (Skauge and Ottesen, 2002; Skauge et al. 2003). About 13 North Sea reservoirs were classified as MWL, MWS or FW, and the different groups showed several important differences with respect to special core analysis properties.

Network models have successfully been used to study the effect of wettability variations on flow at the pore-scale (Mohanty and Salter 1983; Heiba et al., 1983; Kovscek et al. 1993; McDougall and Sorbie 1995; Blunt 1997a,b, 1998; Dixit et al. 1997, 1998,

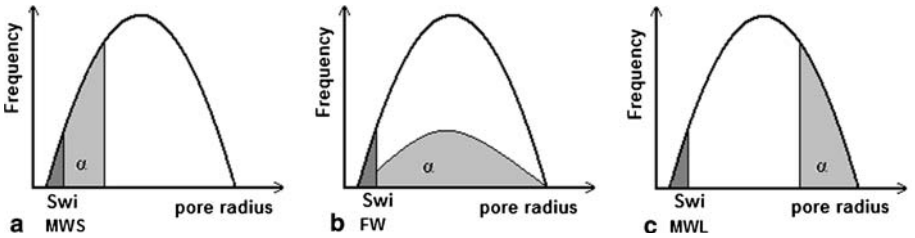

Fig. 1 Distribution of fraction oil-wet pores (α), (**a**) the oil-wet sites are in the small pores, (**b**) random distribution of oil-wet sites and (**c**) oil-wet large pores

Fig. 2 I_{AH} versus I_{USBM} plot which shows the relationship between MWL, MWS and FW (Dixit et al. 1998)

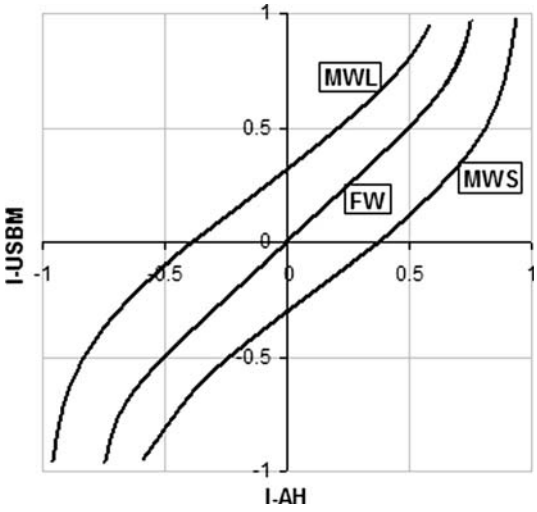

1999, 2000). While these models have progressively captured more of the physics of the pore-scale displacement mechanisms, they have not focused on capturing the complex topology of a reservoir rock. However, recent studies (Jackson et al. 2003; Valvatne and Blunt 2003; Valvatne et al. 2004) have combined a physically based pore-scale model for wettability alteration (Blunt 1998) with a network representation of a Berea sandstone (Bakke and Øren 1997; Øren et al., 1998; Øren and Bakke, 2002, 2003). According to the authors, these models are able to predict experimental relative permeability data for water-wet and mixed-wet rock (Jackson et al. 2003; Valvatne and Blunt 2003; Valvatne et al. 2004).

In this article we are expanding the use of network models to analyse the effect of local wetting parameters such as contact angles, process dependent contact angles, contact angle distribution and fraction of oil-wet sites on fluid flow properties for MWS, MWL and FW wettability classes. The network representation is based on the network model used by Jackson et al. (2003), Valvatne and Blunt (2003) and Valvatne et al. (2004). The results from network simulations are compared with results from experimental core analysis of North Sea cores (Skauge and Ottesen 2002; Skauge et al. 2003).

2 The network model

The network model used in this work is an invasion-percolation code (Valvatne 2004; Valvatne and Blunt 2004), which applies a 3D voxel representation of a Berea sandstone (Bakke and Øren 1997; Øren and Bakke 2003). The network covers a rock volume of 3 mm^3 and involves 28 500 pore elements consisting of pore bodies connected by throats. Most of the pore elements have a cross section form of irregular triangles, however, 6.5% of the pore bodies and throats have a square form and 1.2% have circular cross section form. The average coordination number between pores and throats is 4.19. The porosity and permeability is 18.3% and 3.1 D, respectively, which is in good agreement with the real rock sample used to develop the network (Øren and Bakke 2003).

2.1 Primary drainage

The simulation starts with all the pores and throats being strongly water-wet ($\theta = 0^0$) and 100% saturated with water. Oil then enters the system, representing primary oil migration into a reservoir. This process can be described by invasion percolation theory (Wilkinson and Willemsen 1983). During primary drainage the available pore or throat with the lowest capillary pressure will be filled by oil first, i.e., the pore or throat with the largest radius. A pore is accessible if one of the connecting throats is filled with oil and are connected to the oil source. The capillary entry pressure is

$$P_c = P_o - P_w = \frac{2\sigma_{ow}\cos\theta}{r}, \tag{1}$$

where r is the inscribed radius of the pore or throat (pore element) and θ is the contact angle between pore wall and fluid 1 (water) in presence of fluid 2 (oil). Oil invasion can only occur through piston-like displacement. The primary drainage process continues to irreducible water saturation, Swi. In the network simulations presented in this article, Swi was set equal to 0.24 for all cases, corresponding to a capillary pressure of 66 kPa.

Water will remain as films in the corners of the pores if

$$\theta \leq 90^\circ - \frac{\beta}{2} \tag{2}$$

where β is the angle of the pore corners (Mason and Morrow 1984). θ denotes the critical contact angle for films in the corners and is described by Ma et al. (1996). Thus, the critical contact angle for pores and throats is 45° for square shaped cross sections and 60° for cross sections shaped as equilateral triangles.

2.2 Wettability alteration

After primary drainage, wettability changes are applied to a fraction, α, of the pores invaded by oil. The wettability alteration can be done in three ways; the oil-wet fraction is chosen from the pores with the largest radius (MWL), the smallest of the oil invaded pores are made oil-wet (MWS) or the oil-wet pores are chosen randomly, within the oil invaded pores, uncorrelated to size (FW) (see Fig. 1). Contact angles are chosen for both the water- and oil-wet pores. The physical evolution of the three wetting states is described theoretically by Skauge et al. (2006). Pores with star shaped cross sections will have a higher disjoining pressure in the small pores than in the larger pores. In that case the small pores will reach maximum disjoining pressure first and hence wettability is more easily changed in small pores (MWS).

2.3 Displacement mechanisms during water invasion

There are three distinct types of water displacement mechanisms thoroughly described by Lenormand et al. (1983): piston-like, snap-off and pore-body filling. The pore-body filling mechanism depends on the number of adjacent oil-filled throats. A pore body with coordination number z can be filled by z-1 possible events, $I_1 - I_{z-1}$, each occurring at a separate capillary pressure;

$$P_c = \frac{2\sigma_{ow}\cos\theta_a}{r} - \sigma_{ow}\sum_{i=1}^{n} A_i x_i \tag{3}$$

where θ_a is the advancing contact angle, r is the pore radius, n is the number of connecting oil filled throats, A_i are arbitrary numbers and x_i are random numbers between zero and one. When only one connecting throat contains oil, the mechanism is similar to piston-like advance.

Following primary drainage and wettability alteration, water spontaneously imbibes into water-wet pores. During spontaneous imbibition, pores with the highest P_c are invaded first. This corresponds to the smallest pores. Since snap-off occurs at a lower capillary pressure than piston-type advance (Lenormand et al. 1983; Lenormand and Zarcone 1984), snap-off occurs only when the piston-type advance is impossible for topological reasons.

During snap-off, water advances by swelling of the films left in the pore corners after primary drainage. Since water films only remain in the corners if $\theta \leq 90^\circ - \beta/2$ snap-off can only occur in pores with contact angles that satisfy this criterion. When the advancing corner menisci meet, the interface becomes unstable and leads to snap-off, leaving an oil blob in the centre of the pore or throat. This is in contrast to piston-like displacement which leaves water-wet pores completely water-filled.

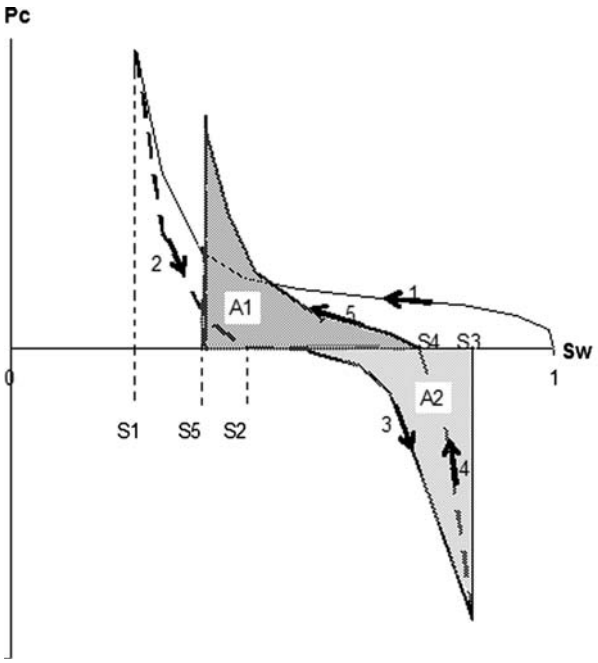

Fig. 3 Capillary pressure curve which shows the imbibition and drainage cycles explored by network simulations

When no more water-wet pores can be spontaneously invaded, the water pressure is increased and water is forced into oil-wet pores. In this case there are two possibilities; the pore or throat can become completely filled with water, or oil may become sandwiched in between water in the corner and water in the centre if

$$\theta \geq 90^\circ + \frac{\beta}{2} \tag{4}$$

It is important to notice that this is a necessary criterion but not a sufficient one as the additional criterion for films is given by geometry (Valvatne and Blunt 2004). Thus, for oil-wet pores with contact angles above 135° (pores with square cross section) or 120° (pores with equilateral triangular cross sections) oil-films will remain in the corners (Ma et al. 1996). With oil-films present it is possible to reach very low oil saturations because of film flow.

2.4 Displacement mechanisms during oil invasion

The last part of the cycle is when oil re-enters the system. For the spontaneous process with $P_c < 0$, the displacement with the highest negative capillary pressure is favoured. Thus, the smallest oil-wet pores will be invaded by oil until zero capillary pressure is reached. During this step, snap-off may occur if the pores contain oil-layers ($\theta \geq 90^\circ + \beta/2$). When all accessible oil-wet pores have been entered, oil pressure has to be increased in order to invade additional pores. Oil is now forced into the network at $P_c > 0$. The oil injection continues until the capillary pressure comes back to the highest value obtained during primary drainage. See Fig. 3 for the full flooding cycle.

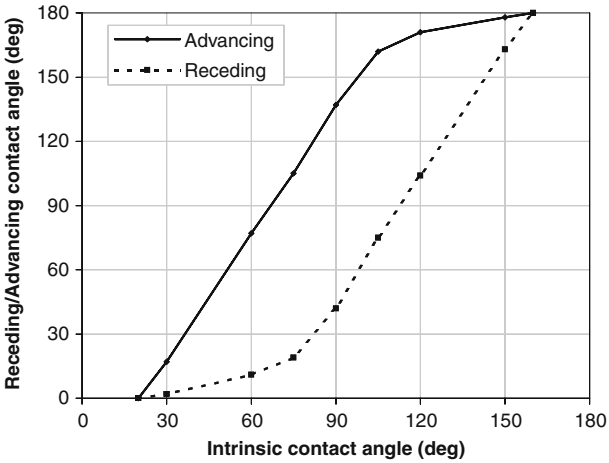

Fig. 4 Advancing and receding contact angles as a function of intrinsic contact angle (Morrow and McCaffery 1976)

2.5 Hysteresis in contact angles

Pores and throats in real porous media have rough surfaces and experience hysteresis between advancing and receding contact angles (Morrow and McCaffery 1976). Advancing contact angles can be seen as increase in water saturation to describe wetting fluid invasion, and receding contact angle describes reduction in water saturation when the wetting fluid is displaced by a non-wetting fluid. If hysteresis is accounted for, each pore must be assigned an intrinsic contact angle in the network model which corresponds to a specific advancing and receding angle, see Fig. 4.

2.6 Wettability indices, Amott–Harvey and USBM

The Amott–Harvey index is based on the Amott wettability indices (Amott 1959), and can be measured through the sequence of displacements described in Sect. 2.3 and 2.4. The water index, I_{w} is defined as;

$$I_{\mathrm{w}} = \frac{\triangle S_{\mathrm{ws}}}{\triangle S_{\mathrm{ws}} + \triangle S_{\mathrm{wf}}} \tag{5}$$

where ΔS_{ws} is the increase in water saturation during spontaneous water imbibition, and ΔS_{wf} is the increase in water saturation during forced water injection. Similarly the oil index, I_{o} is defined as;

$$I_{\mathrm{o}} = \frac{\triangle S_{\mathrm{os}}}{\triangle S_{\mathrm{os}} + \triangle S_{\mathrm{of}}} \tag{6}$$

where ΔS_{os} is the increase in oil saturation during spontaneous oil imbibition, and ΔS_{of} is the increase in oil saturation during forced oil injection. The Amott–Harvey wettability index is then

$$I_{\mathrm{AH}} = I_w - I_o. \tag{7}$$

The water- and oil indices can span from 0 to 1, which leads to a combined Amott-Harvey index, I_{AH}, between -1 (strongly oil-wet sample) and 1 (strongly water-wet sample).

The USBM wettability index is calculated from the water saturation and capillary pressure curve (Donaldson et al. 1969). The USBM index is defined as;

$$I_{\mathrm{USBM}} = \log_{10}\left(\frac{A1}{A2}\right) \tag{8}$$

where A1 is the area under the forced oil drive curve, and A2 is the area under the forced water drive curve. The I_{USBM} is positive for more water-wet samples and negative for the more oil-wet ones. Normally the I_{USBM} lies within the interval -1 to 1 and is therefore often compared with the Amott–Harvey index, however, theoretically it can span from $+\infty$ (strongly water-wet samples) to $-\infty$ (strongly oil-wet samples).

3 Results and discussion

3.1 Effect of fraction oil-wet pores, α

The fraction of oil-wet pores can either be defined as a fraction by number (α_{num}) or as a fraction by volume (α_{vol}). In a network, α has to be higher than a critical value (α_{crit}) for the oil-wet pores to span the network from inlet to outlet.

Consider a simple case with oil-wet contact angles of 180°, and 0° for the water-wet pores. For $\alpha < \alpha_{\mathrm{crit}}$ the oil-wet pores do not span the network, and there is no continuous path from a target pore to the outlet, which is essential for the invasion of water into oil-wet pores. Consequently, most of the oil in these oil-wet pores remains trapped after spontaneous water imbibition, and $I_{\mathrm{o}} = 0$ since there is no spanning oil-wet cluster.

Simulations show that both the critical oil-wet fraction by number ($\alpha_{\mathrm{num,crit}}$) and the critical oil-wet fraction by volume ($\alpha_{\mathrm{vol,crit}}$) is different for the three classes of intermediate wettability. However, the difference between values of $\alpha_{\mathrm{num,crit}}$($\approx 0.3$(MWL), ≈ 0.5(FW), and ≈ 0.7 (MWS)) is larger than between values of $\alpha_{\mathrm{vol,crit}}$ (≈ 0.54(MWL), ≈ 0.5(FW), and ≈ 0.4(MWS)). It should be noted that these results are a consequence of the pore size distribution of the reconstructed Berea network, and are not necessarily applicable to other networks. Figure 5 shows the distribution of Amott–Harvey and USBM indices for the simulations with varying α_{num}, while Fig. 6 gives the relationship between α_{num} and $\alpha_{\mathrm{vol}}$for the three classes of intermediate wettability. In Figure 6, the solid lines show the range of α values were the oil-wet pores span the network. The error in wettability indices is estimated to be ± 0.02 for AH and ± 0.04 for USBM based on series with five repeated experiments.

As expected, $\alpha_{\mathrm{num,crit}} = \alpha_{\mathrm{vol,crit}}$ for the FW class where oil- and water-wet sites are uncorrelated to pore size. For the MWL class $\alpha_{\mathrm{num,crit}} < \alpha_{\mathrm{vol,crit}}$, while for the MWS class it is the opposite with $\alpha_{\mathrm{num,crit}} > \alpha_{\mathrm{vol,crit}}$. The low value of $\alpha_{\mathrm{num,crit}}$for MWL and the high value for MWS can be understood by considering the pore sizes the oil-wet pores are drawn from. For the MWS case, the oil-wet pores are drawn from the small pores, and thus more pores are necessary to form a spanning cluster. The opposite is true for the MWL case where fewer large pores are necessary to form a spanning oil-wet cluster. The relationship between the fraction of oil-wet pores by number and the fraction of oil-wet pores by volume depends on the pore radius and shape. Since the pore volume is often considered to be proportional to the pore radius in some way (depending on the pore shape, see e.g. Øren et al. 1998; Dixit et al. 1999), a few large

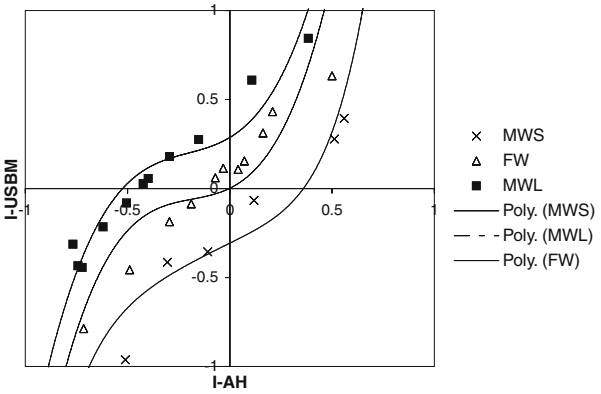

Fig. 5 I_{AH} versus I_{USBM} with contact angles of 0° (water-wet pores) and 180°0 (oil-wet pores). Fraction of oil-wet pores varies between 0 and 1

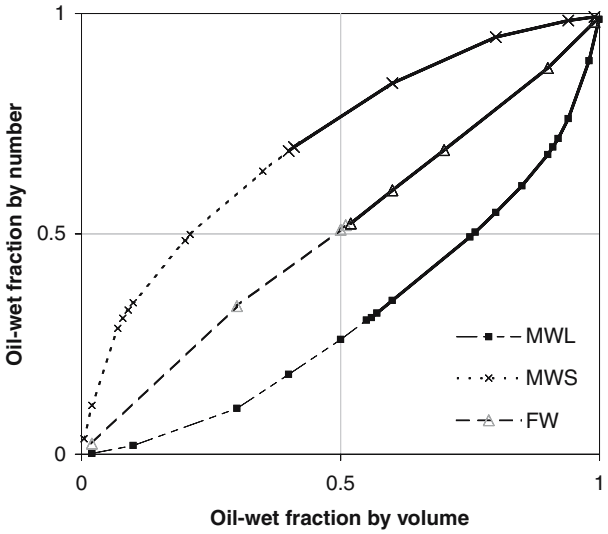

Fig. 6 Relationship between fraction of oil-wet pores by number (α_{num}) and fraction oil-wet pores by volume (α_{vol}) for MWL, MWS and FW. The whole lines show where the oil-wet pores span the Berea network used in the simulations. A contact angle of 180° is used in the oil-wet pores, and 0° for the water-wet pores

oil-wet pores will correspond to a much higher volume fraction than a large number of small oil-wet pores.

Figure 7 shows how Sor varies with α_{vol} for the different wettability classes. The estimated error for Sor values is ±0.02. In agreement with the results obtained by Dixit et al. (1999) for α_{num}, there is a slight increase in Sor with increasing α_{vol} for $\alpha_{vol} < \alpha_{vol,crit}$. This is due to an increasing amount of oil-wet pores from which oil cannot be displaced. When α_{vol} increases above $\alpha_{vol,crit}$, however, the curve shows a drop in Sor, indicating that it is now possible to displace oil from the oil-wet pores through a spanning oil-wet cluster. As α_{vol} increases there are more possible routes by which oil can escape from the network. The piston-type displacement mechanism becomes increasingly important as the number of bypass events decreases, and consequently Sor decreases further. For a given $\alpha_{vol} > 0.5$, Sor increases in the order

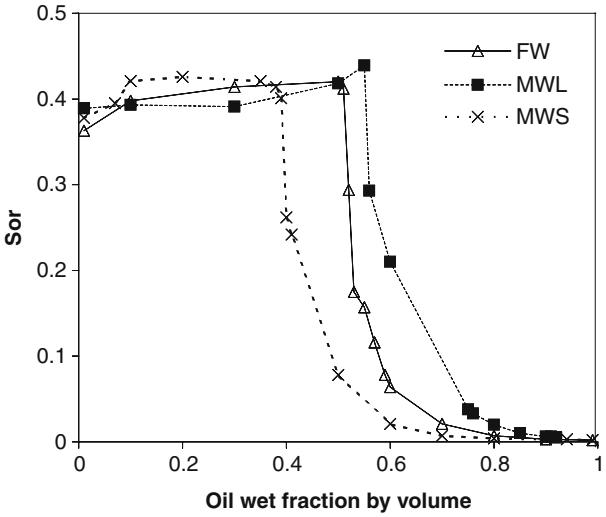

Fig. 7 Residual oil saturation (Sor) as a function of oil-wet fraction by volume for simulations with a contact angel of 0° in the water-wet and 180° in the oil-wet region (case A)

MWS < FW < MWL. The opposite trend in Sor, i.e. Sor increases in the order MWL < FW < MWS, is observed for a given value of $\alpha_{\text{num}} > 0.5$.

3.2 Effect of contact angle

In the analytical work by Dixit et al. (1998), single valued contact angles with no hysteresis were assumed (0° in the water-wet and 180° in the oil-wet pores). The analytical work was confirmed by network modelling, including sensitivities with respect to the contact angle in water-wet pores. The contact angles in the oil-wet pores were uniformly distributed between 91 and 120° in all simulations. In their model, the value of a critical water-wet contact angle (θ_{cw}) establishes whether water invasion can take place by snap-off or not. Similarly, the value of the critical oil-wet angle (θ_{co}) determines whether oil layers can form or not. Snap-off can take place in the range 0° to θ_{cw}, while oil layers only form in the range $\theta_{\text{co}}$to 180°. Values of $\theta_{\text{cw}} = 60°$ and $\theta_{\text{co}} = 120°$ were chosen, which are consistent with an equilateral triangular pore shape (Dixit et al. (1998)). In the network model used in our studies, however, the pore space consists of a variety of irregularly shaped pores. Thus, defining fixed limits for the transition from one pore-scale displacement event to another is not possible. This is likely more representative of the situation in a real porous medium, and in the following sections we discuss the effect of contact angle on wettability indices and Sor in these networks.

In the network model used here, contact angles for the water- and oil-wet pores can be assigned in different ways; as single values, as distributed between an upper and a lower limit and as being process dependent or not, i.e. with or without hysteresis. Process dependent contact angles are allocated using an intrinsic angle, or a distribution of such, which corresponds to a set of advancing and receding angles. The advancing contact angle is always higher than or equal to the receding angle (see Fig. 4).

3.2.1 Single contact angles, no hysteresis

Considering first the case of single valued contact angles with no hysteresis, we find that a contact angle of 0° in the water-wet and 180° in the oil-wet pores reproduces the relationship between I_{AH} and I_{USBM} for the three different wettability classes obtained by Dixit et al. (1998). In the following, this case will be referred to as case A.

When the contact angle in the water-wet pores is increased (0°–80°), the result is lower values of both I_{USBM} and I_{AH}. The effect on the USBM index is by far the largest. Similarly, when the contact angles in the oil-wet pores increase (100°–180°), both wettability indices moves towards lower values. The USBM index is affected the most. The effect of increasing the contact angles in the oil-wet pores is larger than that of increasing the contact angles in the water-wet pores. This may be attributed to our networks having $\alpha_{vol} > 0.55$ i.e. there are more oil-wet than water-wet pores. On the other hand, Valvatne and Blunt (2003) found Sor and the Amott oil index (I_o) to be more affected by the distribution of contact angles in oil-wet pores without constraining this to situations where the fraction of oil-wet pores is larger than 50%.

3.2.2 Uniform distribution of contact angles, no hysteresis

Dixit et al. (1999) found that for networks containing no oil-wet pores, i.e. $\alpha = 0$, the recovery for a weakly water-wet system with contact angles uniformly distributed between 1° and 89°was significantly higher than for a strongly water-wet sample with a contact angle of 0° for all pores. This was attributed to the pore filling sequence being dictated by a non-linear combination of pore radius and contact angle for the case with distributed contact angles (see Eqs.1 and 3). A similar decrease in Sor was found in the present work when a strongly water-wet network was made weakly water-wet by shifting from a contact angle of zero everywhere to a distribution of contact angles between 0° and 89°.

Contrary to the observations made for networks with $\alpha = 0$, networks with $\alpha_{vol} > 0.55$ showed an increase in Sor values when the contact angles in the water- and oil-wet pores were changed from 0°and 180°(case A) to being uniformly distributed between 0° and 89° and 91° and 180° (hereafter referred to as case B), respectively. Figure 8 shows Sor as a function of α_{vol} for the three different wettability classes for case B. Judging from the results obtained for case A, the contact angles in the oil-wet pores is expected to have a larger influence on Sor than the contact angles in the water-wet pores. When the contact angles in the oil-wet pores are changed from 180° (case A) to being uniformly distributed between 91° and 180° (case B), the fraction of oil-wet pores containing oil films after water has displaced oil from the pore centres decreases. Thus, in case B the fraction of pores with the possibility of containing oil films is lower than in case A, where oil films are present in all of the oil-wet pores. As a result, oil can be drained down to lower residual saturations in case A than in case B.

3.2.3 Uniform distribution of contact angles with hysteresis

Simulations with intrinsic contact angles uniformly distributed between 20° and 60° in the water-wet and between 114° and 160° in the oil-wet pores (henceforth referred to as case C) were also performed to evaluate the effect of hysteresis. By choosing these ranges, we ensured that the water advancing angles in the water-wet pores remained

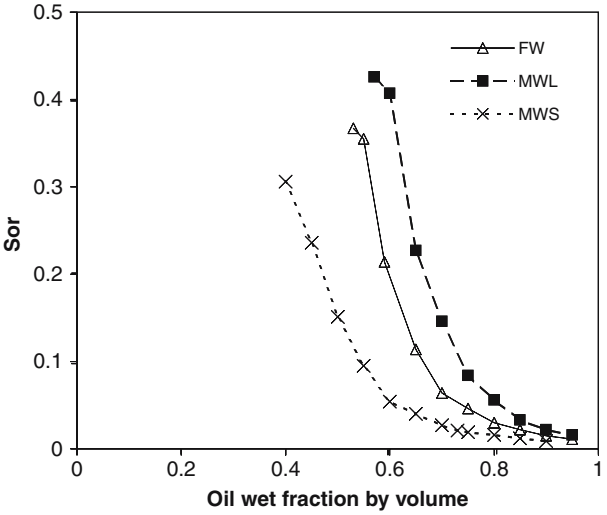

Fig. 8 Residual oil saturation (Sor) for MWL, FW and MWS with uniform distribution of contact angles (case B)

Table 1 Contact angle combinations for case A, B and C

	Case A	Case B	Case C	
θ_{ww}	0°	0°–89°	$\theta_{water,advancing}$	0°–85°
			$\theta_{water,receding}$	0°–10°
θ_{ow}	180°	91° – 180°	$\theta_{oil,advancing}$	170°–180°
			$\theta_{oil,receding}$	95°–180°

below 90° while keeping the water receding angles in the oil-wet pores above 90°. The resulting distributions of water advancing and receding angles in water- and oil-wet pores are listed in Table 1 for case C, along with contact angle combinations for case A and B.

To compare the three different contact angle implementation schemes with respect to their effect on wettability indices and Sor, it is useful to look at each displacement event separately. For the three scenarios discussed, the contact angles in the water-wet pores when water advances during spontaneous imbibition (process 2 in Fig. 3) are 0° (case A), uniformly distributed between 0° and 89° (case B) or uniformly distributed between 0° and 85°(case C). The latter case is the hysteresis case. Figure 9 shows Sor as a function of α_{vol} for the three different wettability classes for case C. Since snap-off is the dominant displacement mechanism for strongly water-wet systems, we expect the volume of water that spontaneously imbibes to be lower in case A than in cases B and C. The two latter cases are assumed to result in quite similar volumes of water imbibed.

During water injection (process 3 in Fig. 3), water advances into oil-wet pores that have contact angles of 180° (case A), angles that are uniformly distributed between 91° and 180° (case B) or uniformly distributed between 170° and 180° (case C). For simplicity, we ignore the possible invasion of water-wet pores that were not invaded after spontaneous water imbibition. At the same fraction of oil-wet pores, Sor is expected to be lower for cases A and C than for case B. This is in accordance with our observations, and due to a decrease in the fraction of oil-wet pores containing oil films after displacement of oil by water. The presence of oil films allows oil to drain down

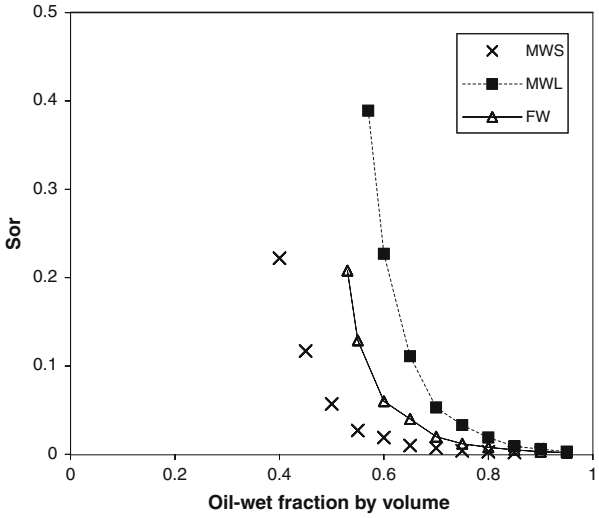

Fig. 9 Residual oil saturation (Sor) for MWL, FW and MWS with uniform distribution of contact angles with hysteresis (case C)

to very low saturations. On the contrary, the area under the forced water injection curve (A2, see Fig. 3) is expected to increase from case B to cases A and C, since the work associated with displacing oil from strongly oil-wet pores is larger than when oil is displaced from more weakly oil-wet pores.

When oil spontaneously imbibes to displace water from oil-wet pores (process 4 in Fig. 3), water recedes from pores that have contact angles of 180° (case A), angles that are uniformly distributed between 91° and 180° (case B) or uniformly distributed between 95° and 180° (case C). The volume of oil that spontaneously imbibes is thus likely to increase from case A to cases B and C, since snap-off can take place in pores with oil films.

When oil is injected to displace water from water-wet pores (process 5 in Fig. 3), water recedes from pores that have contact angles of 0° (case A), angles that are uniformly distributed between 0° and 89° (case B) or uniformly distributed between 0° and 10° (case C). Injection continues until the maximum capillary pressure obtained during primary drainage is reached. Again, in the discussion, injection of oil into oil-wet pores that were not invaded during spontaneous oil imbibition is ignored. Since all our simulations are done using the same network, with contact angles equal to zero everywhere during primary drainage (process 1 in Fig. 3), to obtain the same initial water saturation, the maximum drainage pressure is the same for all simulations. According to Eq. 1, the entry pressure for water-wet pores with a given pore size increases with decreasing contact angle. In secondary drainage, oil injection continues at increasing entry pressures until the maximum entry pressure is reached. Hence, the total volume of oil that can be injected in this step is higher for case B than for cases A and C. In this case, the area under the forced oil injection curve (A1, see Fig. 3) is predicted to be lower for case B than for cases A and C, since the work associated with displacing water from strongly water-wet pores is larger than when water is displaced from weakly water-wet pores.

It follows from the arguments above that the USBM indices for cases A and C should be similar and lower than the USBM index for case B, while the Amott–Harvey indices should increase in the order I_{AH} case A $< I_{\mathrm{AH}}$ case C $< I_{\mathrm{AH}}$ case B.

This is in agreement with the results obtained in the present study. It should be noted that cases A–C all reproduce the order of trendlines found by Dixit et al. (1998) in a plot of I_{USBM} against I_{AH} (i.e. MWS < FW < MWL). This shows that α and type of wettability class is dominating when it comes to trends in wettability indices (I_{AH} versus I_{USBM} plots), and that contact angles are of lesser importance.

3.3 Network simulation versus experimental data- comparison of trends

Comparing results obtained from network modelling studies to experimental results is not straight forward. One important factor that should always be kept in mind is that while displacements in most network models are quasi-static and controlled by capillary forces, experimental waterfloods are dynamic processes that are governed by a combination of viscous and capillary forces. Even though experimental waterfloods are run at low water injection rates, i.e. towards a capillary dominated regime, they are influenced by experimental artefacts through capillary end effects and possibly also viscous rate effects. Capillary end effects are difficult to avoid experimentally, and may lead to artificially high residual oil saturations due to accumulation of oil at the outlet end of the core. In this study, the pore size distribution is kept constant, and capillary forces thus vary due to local wetting properties only. Results obtained for cores, however, are likely influenced by the fact that capillarity varies due to changes in both pore size distribution (permeability and porosity) and local wetting properties.

Since permeability affects capillarity in porous media, it also affects Swi. Furthermore, many experiments have found an increase in Sor with decreasing Swi in a so-called Land-type relationship (Land 1968). In our network modelling studies neither variations in permeability nor Swi were included, and as a result the influence of wettability effects on fluid flow parameters is directly investigated.

Another important issue is related to the question of how porous media wettability is best represented using network models. Which fractions of oil-wet pores should be used? Are single valued contact angles with no hysteresis representative, or should uniformly distributed contact angles with hysteresis be used? Which contact angles or ranges of contact angles is representative of the wettability of water- and oil-wet pores, respectively? Since neither the fraction of oil-wet pores nor the contact angles in different regions of porous media can be determined experimentally, there is no simple answer to these questions. Nevertheless, for the remainder of this discussion we will consider results obtained from case C, i.e. uniform distribution of contact angles with hysteresis.

The permeability of the core samples constituting the experimental data ranged from 14 D to 20 mD (average 2.8 D), while Swi varied from 0.4 to 0.05 (average 0.20). The network models, on the other hand, had a permeability of 3.1 D and Swi equal to 0.24. The work by Valvatne and Blunt (2004) has already shown that the network model can reproduce Sor values, capillary pressure and relative permeability curves. The aim of this article is not to reproduce Sor values or wettability indices, but to show that the trend between the three wettability classes can be reproduced by network modelling. If the trends in experimental data can be reproduced a better understanding of fluid movement for intermediate wet cores will be accomplished.

In the experimental data set Amott–Harvey wettability indices were mainly distributed between −0.5 and 0.5, with the main part of the data having $I_{AH} > 0$ (Skauge et al. 2002), see Fig. 10. A selection of the experimental data from Skauge et al. (2002) has been made. To classify different oil fields according to intermediate wet

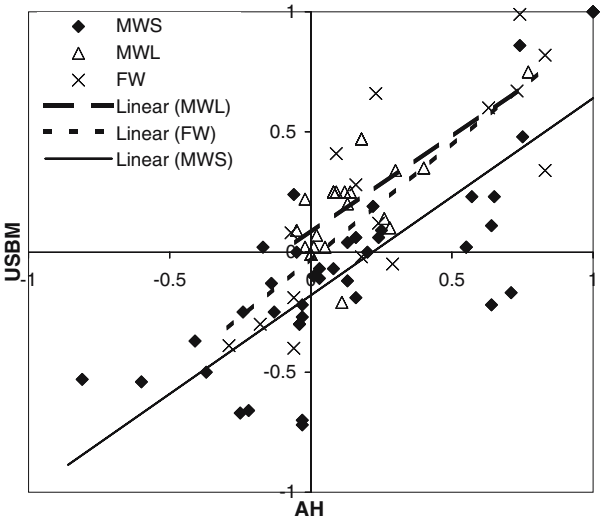

Fig. 10 Experimental data with wettability indices, AH and USBM from eight different fields classified as MWL, FW and MWS (Skauge et al. 2002)

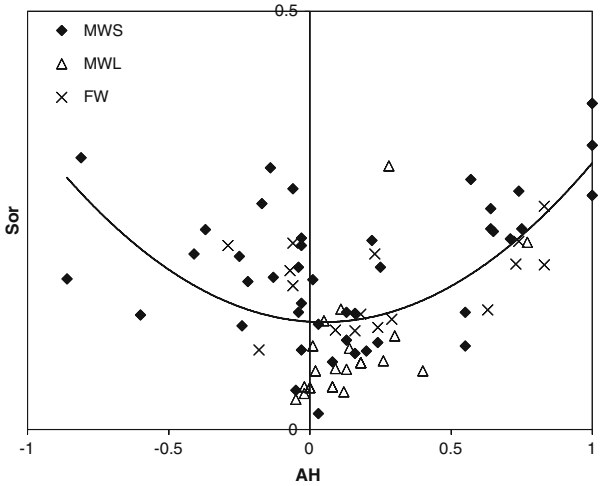

Fig. 11 Experimental data, Sor from eight different oil-fields classified as MWL, FW or MWS based on AH and USBM. The line gives the trend for all data points (Skauge et al. 2002)

class, only datasets with enough data on wettability indices have been included in the comparison towards simulation data. The trend between the AH and USBM indices is the same between the three wettability classes when the experimental results are compared to simulation data (Fig. 5). Experimental results for Sor and normalized end-point relative permeability are given in Figs. 11 and 12. The figures show a large scatter in values, with observed trends; Sor (MWS) > Sor (FW) > Sor (MWL), and MWL > FW > MWS for end-point relative permeability ((1-Sor)*krw(Sor)). As a first approach to comparing network modelling results to experimental results, we thus picked simulations from case C with varying fractions of oil-wet pores that all gave rise to I_{AH} between −0.5 and 0.5. From these simulations, average Sor and normalized end-point relative permeabilities ((1-Sor)*krw(Sor)) were calculated for the different wettability classes. Results for Sor are shown in Fig. 13 and indicate that Sor (MWS) < Sor (FW) < Sor (MWL), contrary to the experimental results shown in

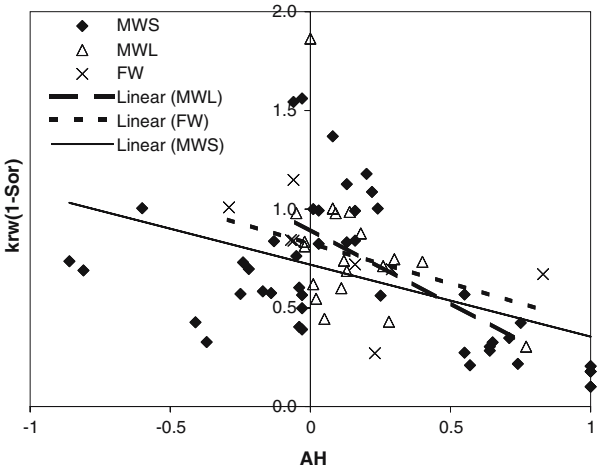

Fig. 12 Experimental data on normalized end-point relative permeability from eight different oil-fields classified as MWL, FW or MWS based on AH and USBM Skauge et al. (2002)

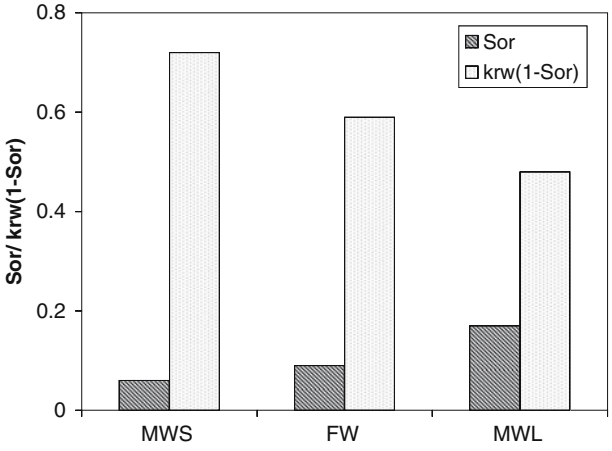

Fig. 13 Average residual oil saturations (Sor) and normalized end-point relative permeability for simulations with IAH between −0.5 and 0.5 shown for a uniform distribution of contact angles with hysteresis, case C (see Table 1)

Fig. 11 (Skauge et al. 2003). Figure 13 shows that the opposite trend is found for the normalized end-point relative permeability.

The comparison of experimental- and network modelling results show that the simulation data predicts too low Sor values for MWS. This suggest that either the experimental data has artificially high values due to end effects during water imbibition, or the simulation data overpredict film flow resulting in very low residual oil saturations. The network simulation data can be manipulated, by cutting the capillary curve at a lower absolute pressure, resulting in higher Sor values. By doing this the film flow will be suppressed and the Sor results become more comparable to the experimental recoveries, see Fig. 14. In the same operation the normalized end-point relative permeability can be estimated from the cut capillary pressure, see Fig. 15.

The average Sor and normalized end-point relative permeability can be recalculated from the results in Figs. 14 and 15. Only the simulations with AH between

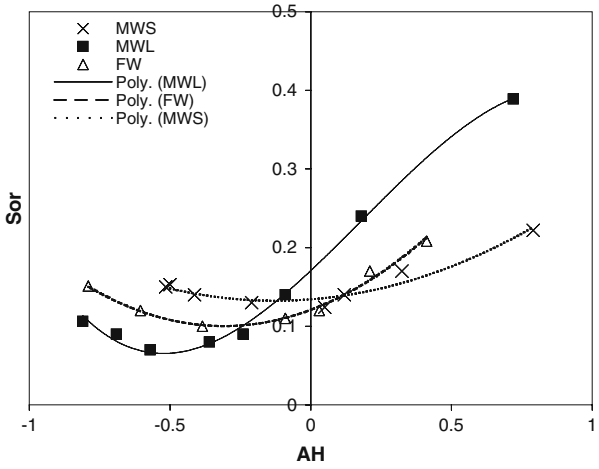

Fig. 14 Manipulated Sor values from network simulations as a function of AH shown for a uniform distribution of contact angles with hysteresis, case C (see Table 1)

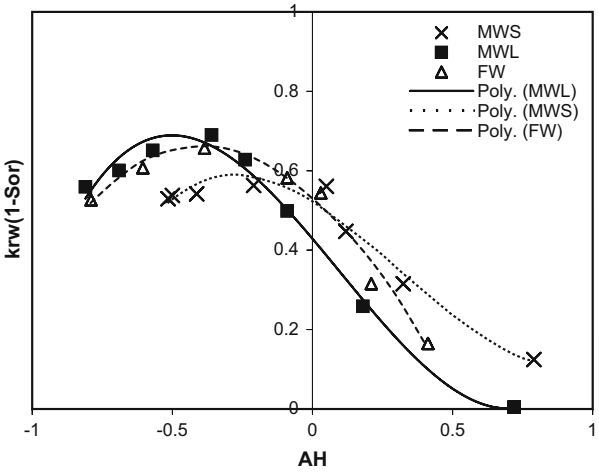

Fig. 15 Manipulated normalized end-point relative permeability values for network simulations as a function of AH. The distribution of contact angles is uniform with contact angle hysteresis, case C (see Table 1)

−0.5 and 0.5 are included in the new average values. When comparing the Sor from experimental studies with the simulation results Fig. 16 shows that the trend is consistent between the three wettability classes. The same holds for normalized end-point relative permeability in Fig. 17.

The difference in trends between the original network modelling studies and experimental data indicate that wettability effects, when considered in isolation, cannot fully explain the variations in residual oil saturation and end-point relative permeabilities. By manipulating the simulation data to make them comparable to the experiments, the results give the same trends between the three wettability classes for both experimental and simulation data. It is important to note that Sor depends on many factors i.e. porosity, permeability, Swi and so on, so a full explanation on the variation in Sor cannot be obtained from simulations which only look at different wetting scenarios. The results presented here have nevertheless shown that trends between the wettability classes can be reproduced.

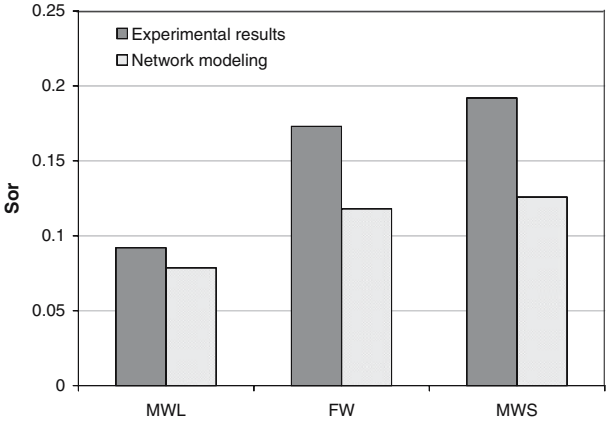

Fig. 16 Comparison of average experimental Sor results (Skauge et al. 2003) and average Sor values from manipulated simulation data

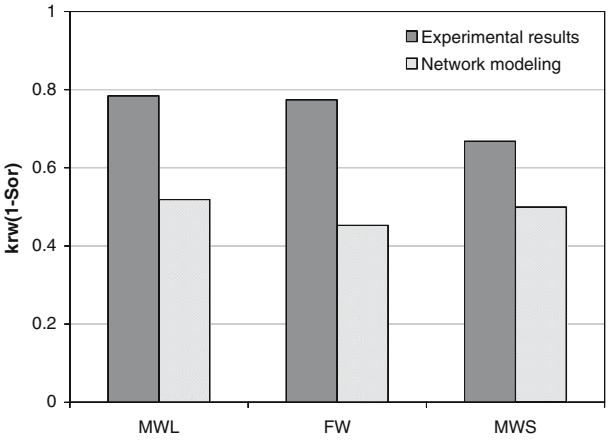

Fig. 17 Comparison of average experimental results on normalized end-point relative permeability (Skauge et al. 2003), with average from manipulated simulation data

4 Conclusions

A pore reconstruction model is used to investigate effects of local wetting parameters on fluid flow properties. The results from network simulations confirm the trends of wettability indices I_{USBM} and I_{AH} for the intermediate wetting classes, MWL, FW and MWS.

When the contact angles in the oil-wet pores are changed from 180° to being uniformly distributed between 91° and 180°, the fraction of oil-wet pores containing oil films after water has displaced oil from the pore centres decreases. As a consequence oil can be drained down to lower residual saturations in the case with constant contact angle than in the case with distributed contact angles.

The network model reproduces the trend in wettability indices observed from experimental data. Experimental results have shown variation in residual oil saturation as a function of type of intermediate wettability. With a modification of the data from the network model the same trend in Sor, with respect to wettability class, is seen in both simulation and experimental results.

One important factor that should always be kept in mind is that while displacements in most network models are quasi-static and controlled by capillary forces,

experimental waterfloods are dynamic processes that are governed by a combination of viscous and capillary forces. It is also important to remember that Sor is a function of many variables. In this work, local wetting properties has been isolated and a trend in Sor data has been confirmed, though it cannot fully explain all variations in Sor.

References

Amott, E.: Observations relating to the wettability of porous rocks. Trans AIME. **216**, 156–162 (1959)

Bakke, S., Øren, P.E.: 3D Pore-Scale Modelling of Sandstones and Flow Simulations in the Pore Networks. SPE J. **2**, 136–149 (1997)

Blunt, M.J.: Effects of heterogeneity and wetting on relative permeability using pore level modeling. SPE J. **2**, 70–86 (1997a)

Blunt, M.J.: Pore level modeling of the effects of wettability. SPE J. **2**, 494–510 (1997b)

Blunt, M.J.: Physically-based network modelling of multiphase flow in intermediate-wet porous media. J. Petrol. Sci. Eng. **20**, 117–125 (1998)

Boneau, D.F., Clampitt, R.L.: A Surfactant system for the oil-wet sandstone of the North Burbank Unit. J. Petrol. Technol. May, 501–506 (1977)

Dixit, A.B., McDougall, S.R., Sorbie, K.S.: A Pore-Level Investigation of Relative Permeability Hysteresis in Water-Wet Systems, Paper presented at the SPE International Symposium on Oilfield Chemistry, held in Houston, Texas, 18-21 February, SPE paper 37233 (1997)

Dixit A.B., Buckley J.S., McDougall S.R., Sorbie K.S.: Core wettability: Should I_{AH} Equal I_{USBM}? Paper presented at the International Symposium of the SCA, the Hague, the Netherlands, September (1998)

Dixit, A.B., McDougall, S.R., Sorbie, K.S., Buckley, J.S.: Pore-Scale modelling of wettability effects and their influence on oil recovery. SPE Reservoir Eval. Eng. **2**(1), 25–36 (1999)

Dixit, A.B., Buckley, J.S., McDougall, S.R., Sorbie, K.S.: Empirical measure of wettability in porous media and the relationship between them derived from pore-scale modeling. Transport Porous Med. **40**, 27–54 (2000)

Donaldson, E.C., Thomas, R.D., Lorenz, P.B.: Wettability determination and its effect on recovery efficiency. SPE J. March, 13–20 (1969)

Heiba, A.A., Davis, H.T., Scriven, L.E.: Effect of Wettability on Two-Phase Relative Permeabilities and Capillary Pressures, Paper presented at the 58th Annual Technical Conference and Exhibition held in San Francisco, CA, October 5-8, SPE paper 12172 (1983)

Jackson, M.D., Valvatne, P.H., Blunt, M.J.: Predictions of wettability variation and its impact on flow using pore- to reservoir-scale simulations. J. Petrol. Sci. Eng. **39**, 231–246 (2003)

Kovscek, A.R., Wong, H., Radke, C.J.: A Pore-Level Scenario for the Development of Intermediate wettability in Oil Reservoirs. AlChE J. **39**(6), 1072–1085 (1993)

Land, C.S.: Calculation of Imbibition relative permeability for two-and three-phase flow from rock properties. SPE J. June, 149–156 (1968)

Lenormand, R., Zarcone, C., Sarr, A.: Mechanisms of the displacement of one fluid by another in a network of capillary ducts. J. Fluid Mech. **135**, 337–353 (1983)

Lenormand, R., Zarcone, C.: Role of roughness and edges during imbibition in square capillaries, Presented at the SPE Annual Technical Conference and Exhibition, 16-19 September, Houston, Texas, SPE paper 13264 (1984)

Ma, S., Mason, G., Morrow, N.R.: Effect of contact angle on drainage and imbibition in regular polygonal tubes. Colloid. Surf. A: Physicochem Eng. Aspect. **117**, 273–291 (1996)

Mason, G., Morrow, N.R.: Meniscus Curvatures in Capillaries of Uniform Cross-section. J. Chem. Soc. Faraday Trans. 1 **1**(80), 2375–2393 (1984)

McDougall, S.R., Sorbie, K.S.: The impact of wettability on water flooding: Pore-scale simulation. SPE Reservoir Eng. **10**(3), 208–213 (1995)

Mohanty, K.K., Salter, S.J.: Multiphase Flow in Porous Media: III. Oil Mobilization, Transverse Dispersion, and Wettability, Paper presented at the 58^{th} Annual Technical Conference and Exhibition held in San Francisco, CA, October 5-8, SPE paper 12127 (1983)

Morrow, N.R., McCaffery, F.G.: Displacement Studies in Uniformly Wetted Porous Media, Society of Chemical Ind. International symposium on wetting, Loughborough, England, 21–29 September (1976)

Øren, P.E., Bakke, S., Arntzen, O.J.: Extending predictive capabilities to network models. SPE J. December, 324–336 (1998)

Øren, P.E., Bakke, S.: Process based reconstruction of sandstones and prediction of transport properties. Transport Porous Med. **46**, 311–343 (2002)
Øren, P.E., Bakke, S: Reconstruction of Berea sandstone and pore-scale modelling of wettability effects. J. Petrol. Sci. Eng. **39**, 177–199 (2003)
Skauge, A., Ottesen, B.: A Summary of Experimentally derived Relative Permeability and Residual Saturation on North Sea Reservoir Cores, Paper presented at the International Symposium of the SCA, Monterey, CA, September (2002)
Skauge, A., Ottesen, B., Vik, B.: Variation of Special Core Analysis Properties for Intermediate Wet Sandstone Material, Paper presented at the International Symposium of the SCA, Pau, France, September (2003)
Skauge, A., Spildo, K., Høiland, L., Vik, B.: Theoretical and experimental evidence of different wettability classes. J. Petrol. Sci. Eng. in press (2006)
Valvatne, P.H., Blunt, M.J.: Predictive Pore-Scale Network Modeling, Paper presented at the SPE Annual Technical Conference and Exhibition held in Denver, Colorado, USA, 5–8 October, SPE paper 84550 (2003)
Valvatne, P.H., Jing, X.D., Smits, R.M.M.: (2004), Modeling Pore Geometric and Wettability Trends of Multiphase flow in Porous Media, Paper Presented at the International Symposium of the Society of Core Analysts held in Abu Dhabi, UAE, 5–9 October
Valvatne, P.H.: Predictive Pore-Scale Network Modeling, PhD thesis, Imperial college, London, England (2004)
Valvatne, P.H., Blunt, M.J.: Predictive pore-scale modeling of two-phase flow in mixed wet media. Water Resour. Res. **40**, W07406, doi:10.1029/2003WR002627 (2004)
Wilkinson, D., Willemsen, J.F.: Invasion percolation: a new form of percolation theory. J. Phys., A: Math. Gen **16**, 3365–3376 (1983)